Contrail formation in aircraft wakes using large-eddy simulations

By   R. Paoli †, J. Hélie ‡, T. J. Poinsot ¶ AND S. Ghosal ∥

In this work we analyze the issue of the formation of condensation trails ("contrails") in the near-field of an aircraft wake. The basic configuration consists in an exhaust engine jet interacting with a wing-tip trailing vortex. The procedure adopted relies on a mixed Eulerian/Lagrangian two-phase flow approach; a simple micro-physics model for ice growth has been used to couple ice and vapor phases. Large eddy simulations have carried out at a realistic flight Reynolds number to evaluate the effects of turbulent mixing and wake vortex dynamics on ice-growth characteristics and vapor thermodynamic properties.

1. Introduction

Contrails are ice clouds generated by water in the exhaust from aircraft engines, forming the common visible white lines in the sky. As assessed in the special report of the Intergovernmental Panel on Climate Change (IPCC report (1999)), they have an important environmental impact because they artificially increase cloudiness and trigger the formation of cirrus clouds, thus altering climate both on local and regional/global scales (see figure 1). This was confirmed in a recent climate study (Travis *et al.* (2002)) performed in the three days following the 11th of September 2001, when all american aircraft were grounded and there were no contrails over the USA. During this period, abnormal and significant temperature differences between day and night (namely, "daily temperature range" or DTR) were observed in the USA. This confirms that contrails are of major importance for global climate change by artificial clouds formation.

Contrails consist of ice crystals which form mainly by condensation of exhaust water vapor over suitable nucleation sites, like soot particles and sulfur aerosols, emitted by aircraft engines (Schumann (1996), Karcher & *al.* (1996)). Background atmospheric vapor, which eventually adds to the exhaust content, is responsible for the persistence of contrails (Gierens (1996)). Contrails form when the air surrounding a nucleation site becomes supersaturated with respect to ice (Appleman (1953), Schumann (1996)). For certain atmospheric conditions, this may occur somewhere in the jet plume, as the result of the increased humidity due to mixing between hot and moist exhaust gases with cold and less humid ambient air. In a temperature/vapor-pressure plane (see figure 2), assuming that vapor and heat diffuse at the same rate ($(Sc = Pr)$ and that the flow is adiabatic, pure mixing can be graphically represented by a straight ("mixing") line which is completely defined by the two states A (ambient air) and B (exhaust gas). In figure 2, supersaturation corresponds to the thermodynamic states lying between S_1 and

† CERFACS
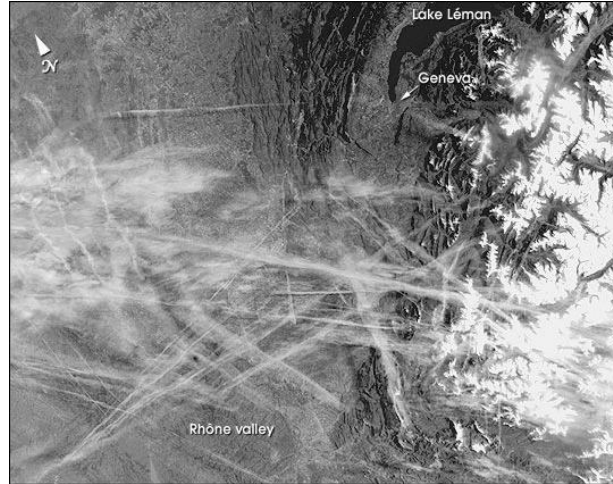‡ IMFT
¶ CERFACS and IMFT
∥ Northwestern University

FIGURE 1. Contrails in South-Eastern France sky (http://eol.jsc.nasa.gov).
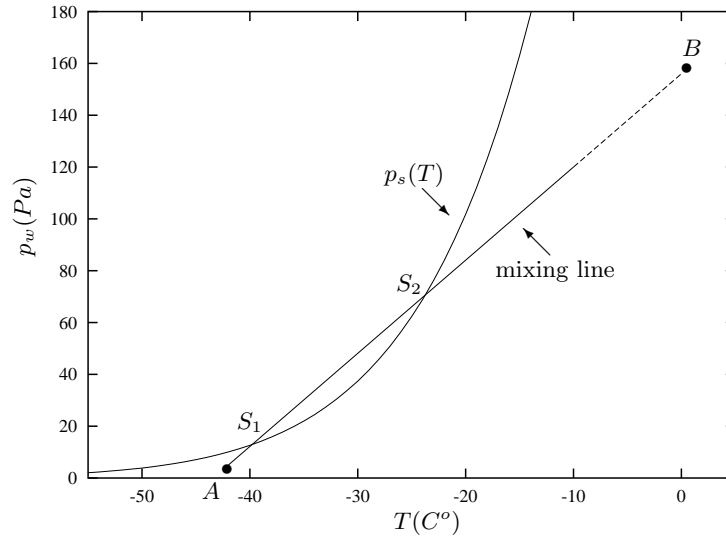

PSfrag replacements

FIGURE 2. Thermodynamic conditions for ice formation: $p_s(T)$ is the saturation curve with respect to ice. State A represents (cold) atmospheric conditions; state B, (hot) exhaust conditions (for the sake of representation, we placed it much closer to p_s than what it really is). States S_1 and S_2 define the range of supersaturation, $p_w > p_s(T)$.

S_2, where $p_w > p_s(T)$. An ice crystal forms when such a condition is locally satisfied in the jet plume and, at the same time, a nucleation particle is present. A two-phase flow solver, using a Lagrangian solver for nucleation particles, then represents the most suitable approach to deal with ice formation in the contrails.

Formation and persistence of contrails have been studied during last years, mostly in geophysical and atmospheric science literature, through *in situ* measurements and numerical simulations with different level of complexity (see IPCC report (1999) and references therein). The main intent there was to characterize the general features of the phenomenon on time scales up to minutes from the emission time. Other authors

investigated in detail the micro-physics of ice formation (the initial composition of the jet contrail, the mechanism of water uptake on the nucleation site, homogeneous versus heterogeneous nucleation, etc. see Pruppacher & Klett (1997) for a complete review).

In the present work we have focused on the simulation of contrail formation and early-stage evolution in the near-field of an aircraft wake, i.e., up to a few seconds from the emission time. The basic configuration consists of an exhaust jet interacting with a wing-tip trailing vortex. This represents a complex issue because of the different phenomena involved, such as jet and wake-vortex instabilities, transition to turbulence, two-phase flow and ice micro-physics. Large-eddy simulations are well suited to deal with all these inherently unsteady processes, at realistic flight Reynolds numbers, and have been used in this work. The object of the study is two-fold. First, we aim to characterize: (i) the spatial distribution of supersaturation around particles, in the jet plume; and (ii) the effects of wake vortex. Then, we test a simple micro-physics model for ice-growth to account for (iii) the early stage of contrail evolution and (iv) its influence on the thermodynamic properties of water vapor. Governing equations for the two-phase flow model are detailed in section 2, results are presented in section 3. In section 4 an alternative approach is proposed to account for a general (initial) distribution of soot particles.

2. Governing equations and ice micro-physics model

Large-eddy simulations of ice formation are carried out through an Eulerian/Lagrangian two-phase flow approach. For the gaseous (carrier) phase we solve fully-compressible Navier-Stokes equations together with a transport equation for a scalar field, representing the exhaust water vapor, Y_w. These equations are filtered spatially so that any variable $\phi(x) = [\rho, \rho\,u, \rho\,v, \rho\,w, \rho\,E, \rho\,Y_w]$ is decomposed into a resolved part $\overline{\phi(x)}$ and a non-resolved (or subgrid-scale) part $\phi''(x)$, with $\phi(x) = \overline{\phi(x)} + \phi''(x)$. For compressible flows, we use Favre-filtered variables, defined as $\phi(x) = \tilde{\phi}(x) + \phi'(x)$, with $\tilde{\phi} = \overline{\rho\phi}/\overline{\rho}$. Using this approach, dimensionless Favre-averaged equations are

$$\frac{\partial \overline{\rho}}{\partial t} + \frac{\partial (\overline{\rho}\tilde{u}_j)}{\partial x_j} = \dot{\omega}, \tag{2.1}$$

$$\frac{\partial (\overline{\rho}\tilde{u}_i)}{\partial t} + \frac{\partial (\overline{\rho}\tilde{u}_i\tilde{u}_j)}{\partial x_j} + \frac{\partial \overline{p}}{\partial x_i} = \frac{1}{Re}\frac{\partial \tilde{\tau}_{ij}}{\partial x_j} + \frac{\partial \sigma_{ij}}{\partial x_j}, \tag{2.2}$$

$$\frac{\partial (\overline{\rho}\tilde{E})}{\partial t} + \frac{\partial [(\overline{\rho}\tilde{E} + \overline{p})\tilde{u}_j]}{\partial x_j} = \frac{1}{Re}\frac{\partial \tilde{\tau}_{ij}\tilde{u}_i}{\partial x_j} + \frac{\partial \sigma_{ij}\tilde{u}_i}{\partial x_j} - \frac{1}{Re\,Pr}C_p\frac{\partial \tilde{q}_j}{\partial x_j} - \frac{\partial Q_j}{\partial x_j}, \tag{2.3}$$

$$\frac{\partial (\overline{\rho}\tilde{Y}_w)}{\partial t} + \frac{\partial (\overline{\rho}\tilde{Y}_w\tilde{u}_j)}{\partial x_j} = \frac{1}{Re\,Sc}\frac{\partial}{\partial x_j}\left(\mu\frac{\partial \tilde{Y}_w}{\partial x_j}\right) + \frac{\partial \xi_j}{\partial x_j} + \dot{\omega}. \tag{2.4}$$

The sub-grid scale (SGS) stress tensor $\sigma_{ij} = -(\overline{\rho u_i u_j} - \overline{\rho}\tilde{u}_i\tilde{u}_j)$, the SGS heat flux $Q_j = \overline{\rho C_p T u_j} - \overline{\rho}C_p\tilde{T}\tilde{u}_j$ and the SGS scalar flux $\xi_j = -(\overline{\rho Y_w u_j} - \overline{\rho}\tilde{Y}_w\tilde{u}_j)$ are modeled through the subgrid-scale eddy-viscosity concept

$$\sigma_{ij} - \frac{1}{3}\sigma_{kk}\delta_{ij} = -2\mu_{sgs}\left(\tilde{S}_{ij} - \frac{1}{3}\delta_{ij}\tilde{S}_{kk}\right), \; Q_j = -\frac{\mu_{sgs}\,C_p}{Pr_t}\frac{\partial \Theta}{\partial x_j}, \; \xi_j = -\frac{\mu_{sgs}}{Sc_t}\frac{\partial \tilde{Y}_w}{\partial x_j}, \tag{2.5}$$

where $\Theta = \tilde{T} - \frac{1}{2\overline{\rho}C_v}\sigma_{kk}$ is the modified temperature (Métais & Lesieur (1992)) while turbulent Prandtl and Schmidt numbers are assumed to be constant. In the present simulations, we assumed $Pr_t = 0.3$ and $Sc_t = 0.3$. Sub-grid scale viscosity μ_{sgs} is obtained

through the Filtered Structure Function model (Métais & Lesieur (1992), Ducros & al. (1996)), initially developed in spectral space and then transposed into physical space. This model was found to be well suited for the simulation of transitional flows, due to the property of insuring no SGS viscosity when there is no energy at the cutoff wavelength (Ducros & al. (1996)). Vapor/ice mass coupling in the continuity and scalar equations, $\dot{\omega}$ is discussed in the next section.

2.1. *Particles treatment and ice-growth model*

Soot-ice particles are tracked through a Lagrangian solver with point force approximation (see Boivin & al. (1998) for details). Due to their small size (from tens of nanometers to a few microns, see Karcher & al. (1996)) their relaxation time is negligible compared to the characteristic times of the filtered gas variables. This allows them to be treated as tracers. In addition, due to their high number density (varying approximately between 10^9 and $10^{11}\,m^{-3}$ (Karcher & al. (1996)), we can carry only packets of particles, or "numerical particles", each one containing a large number n_{trans} of real soot-ice kernels. A numerical particle is defined as the center of mass, $\underline{x}_p$, of n_{trans} physical particles. In the tracer limit, its motion is completely described by

$$\frac{d\underline{x}_p}{dt} = \tilde{\underline{u}}(\underline{x})\,\delta(\underline{x} = \underline{x}_p) \tag{2.6}$$

where $\tilde{\underline{u}}$ is the (filtered) gas velocity. Using filtered quantities instead of exact un-filtered ones is equivalent to neglecting sub-grid dispersion, compared to the resolved, large-scale dispersion. This assumption is justified because the Reynolds number is high. Gas sources are estimated at the numerical particle positions; afterwards they are projected on the Eulerian grid, inversely proportional to the mesh-point distance. This numerical method can be viewed as a spatial filtering (Boivin & al. (1998), Hélie & al. (2002)). Exchange between phases is allowed by the code (two-way coupling). Nevertheless, due to the tracer limit and solid/gas mass ratio, drag momentum exchange is negligible. Temperature cannot be modified by ice growth by more than a few Kelvin (Schumann (1996)), so that thermal coupling is also neglected. Therefore, we only consider mass exchange, i.e. vapor condensation on the soot particle. The term $\dot{\omega}$ can be neglected in (2.1) because of the small amount (order of a few percent) of water vapor in the exhaust gases. On the other hand, in (2.4) it accounts for vapor/ice phase exchange and is related to the rate of growth of a single ice crystal, through the quasi-stationary model (Karcher & al. (1996))

$$\frac{dr_p}{dt} = \frac{J_w}{\tilde{\rho}S_p}, \tag{2.7}$$

$$\dot{\omega} = -\sum_{p=1}^{n_p}\delta(\underline{x} = \underline{x}_p)n_{trans}\frac{dr_p}{dt}\rho_p\,S_p. \tag{2.8}$$

$S_p = 4\pi r_p^2$ and ρ_p are the area of the particle (supposed spherical) and its density, while J_w is the mass flux of water vapor on the particle surface

$$J_w = 4\pi r_p D\,G(r_p)(\tilde{Y}_w - Y_s) \tag{2.9}$$

where $D = \mu/(\rho Sc)$ is the molecular diffusivity of water vaporin air, Y_s is the mass fraction of gaseous water at ice saturation. The dimensionless collision factor $G(r_p)$ is
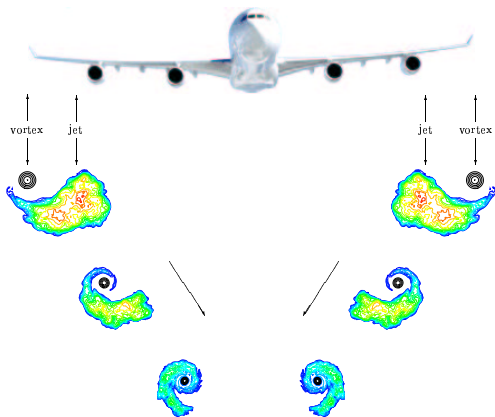
FIGURE 3. Basic configuration of a jet/vortex interaction in the near-field of an aircraft wake.
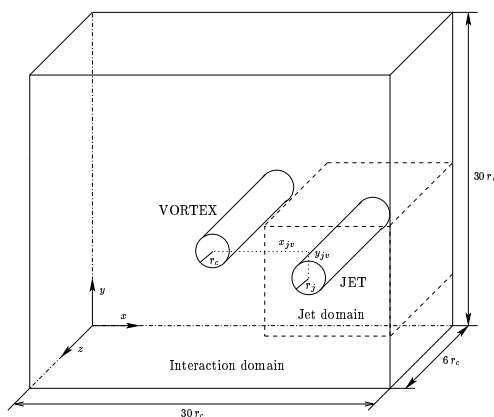

FIGURE 4. Sketch of the computational domains for the jet and the interaction phases.

given by the semi-theoretical correlation

$$G(r_p) = \left(\frac{1}{1 + K_n} + \frac{4K_n}{3\alpha} \right)^{-1}. \tag{2.10}$$

It depends on the Knudsen number $K_n = \lambda/r_p$ (ratio of the vapor mean free path to the particle radius) and the empirical constant $\alpha = 0.1$, and was found to give good results for quasi-isothermal flows and cases with low heat transfer (see Qu & Davis (2001) for details). Saturation conditions are estimated by Sonntag (1994) as

$$p_s = p\, X_s = \exp\Big(\frac{6024.5282}{\tilde{T}} + 29.32707 + 1.0613868\,10^{-2}\,\tilde{T}$$
$$-1.3198825\,10^{-5}\,\tilde{T}^2 - 0.49382577\,\ln\tilde{T}\Big) \tag{2.11}$$

where $\tilde{T}$ is the filtered gas temperature (heat inertia of particles is neglected). Mass and molar fractions at saturation conditions are related by $Y_s = X_s/(X_s+(1-X_s)\,W_{air}/W_w)$, with $W_{air} = 28.85$ kg/Kmole, $W_w = 18.01$ kg/Kmole.

The numerical code, NTMIX3D, is a three-dimensional, two-phase flow, finite-difference solver. For the gas phase, space discretization is performed by a sixth-order compact scheme (Lele (1992)). Time integration is performed by means of a three-stage Runge-Kutta method, for both the two phases. The solver is fully parallel, using domain decomposition. Simulations are performed using 16 processors on CINES O3000 machine.

3. Results

This section describes the results of the simulation of ice formation in the near-field of an aircraft wake. The basic configuration is an exhaust jet interacting with a (single) wing-tip trailing vortex (Fig 3). We adopted a two-stage simulation which consists in first simulating a temporally-evolving jet ("jet phase") and then its interaction with the vortex ("interaction phase"). This procedure has been used previously (Paoli & *al.* (2002), Garnier & *al.* (2002)) and its validity has been recently discussed by some of the authors (Paoli & *al.* (2002)). A sketch of the computational domain for the two phases is shown in figure 4. For the jet phase it has dimensions $L_x = L_y = 16\,r_j$ and $L_z = 6\,r_j$
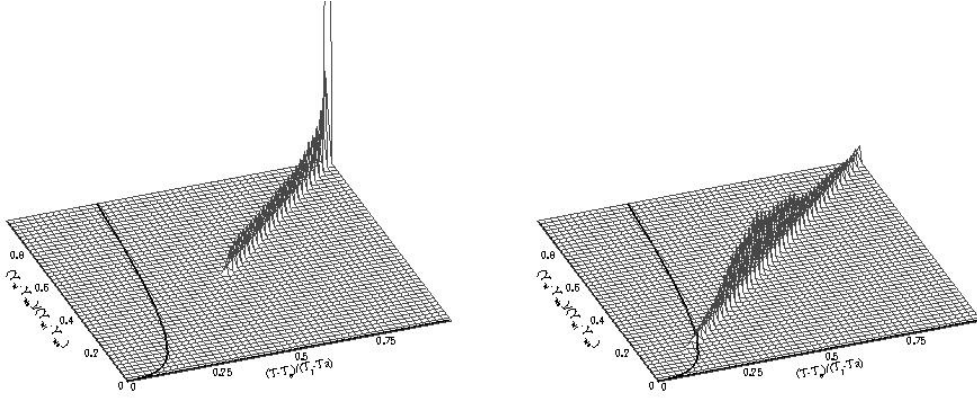
FIGURE 5. Joint PDF of temperature and water vapor partial pressure around passive
particles, during the jet phase (saturation curve is also displayed); left, $t = 0.16\,s$; right
$t = 0.56\,s$.

(z being the jet axis and r_j the exhaust jet radius) and consists of $161 \times 161 \times 61$ grid
points; for the interaction phase, the dimensions are $L_x = L_y = 30\,r_j$ and $L_z = 6\,r_j$ with
$301 \times 301 \times 61$ grid points. The Reynolds number, based on the radius, $r_j = 1\,m$, and the
exhaust jet velocity, $w_j = 60\,\mathrm{m/s}$, is $Re_j = 3.2 \times 10^6$, while the exhaust Mach number is
$M_j = 0.2$. Axial velocity, temperature and vapor mass fraction are initialized according
to a tanh law (for simplicity, all bars and tildes are omitted)

$$w_0(r) = \frac{1}{2}\Big[(w_j + w_a) - (w_j - w_a)\,F(r)\Big]; \quad F(r) = \tanh\left[\frac{1}{4}\frac{r_j}{\theta}\left(\frac{r}{r_j} - \frac{r_j}{r}\right)\right] \qquad (3.1)$$

where r is the radial distance from the center; $r_j/\theta = 10$; while subscripts j and a
indicate exhaust jet and ambient air, respectively (see Paoli & *al.* (2002) for details).
Initial temperature and water vapor mass fraction follow the same law

$$T_0(r) = \frac{1}{2}\Big[(T_j + T_a) - (T_j - T_a)\,F(r)\Big], \qquad (3.2)$$

$$Y_{w_0}(r) = \frac{1}{2}\Big[(Y_{w_j} + Y_{w_a}) - (Y_{w_j} - Y_{w_a})\,F(r)\Big]. \qquad (3.3)$$

In the present simulations we assume no coflow, $w_a = 0$, and no background water
content, $Y_{w_a} = 0$; the exhaust water content, taken from available data (Garnier & *al.*
(1997)), is $Y_{w_j} = 0.03$. Ambient temperature is $T_a = 225\,K$ and exhaust-to-ambient
temperature ratio is $T_j/T_a = 2$ which gives $T_j = 450\,K$, a reasonable value for the
exhaust temperature. The jet is loaded with $n_p = 250000$ (numerical) soot particles with
the same radius $r_p = 0.02\,\mu m$. They behave as tracers and each one represents a packet of
$n_{trans} = 10^6$ physical particles. Particle number density is then 2.5×10^{11}, in agreement
with literature data (Karcher & *al.* (1996)).

A random-noise perturbation δw is added to the base flow w_0 in (3.1) (with $\delta w_{max} =
0.005\,w_0(r)$), to trigger jet instability and transition to turbulence. When the maximum
jet velocity has decreased to half the initial value, the domain is enlarged and a vortex
inserted (the relative position is $x_{jv} = 5\,r_j$ and $y_{jv} = -r_j$, see figure 4), according to the
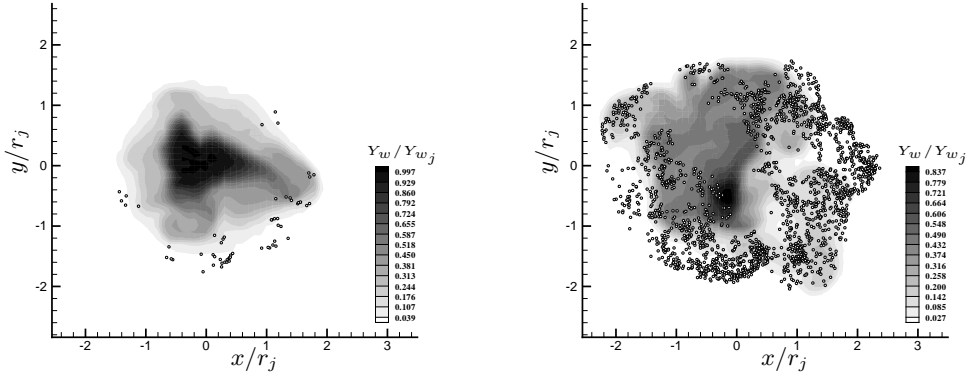
FIGURE 6. Passive particles case (jet phase). Plane cut of vapor content and distribution of supersaturated particles; left, $t = 0.56\,s$; right, $t = 0.7\,s$.

Lamb-Oseen model ($\alpha = 1.4$, $\beta = 1.2544$)

$$v_\theta(r) = \alpha\, v_c \frac{r_c}{r} \left\{ 1 - exp\left[-\beta \left(\frac{r}{r_c} \right)^2 \right] \right\}; \qquad \frac{dp}{dr} = \rho \frac{v_\theta^2}{r} \tag{3.4}$$

where $r_c = r_j$ is the vortex core radius and $v_c = 1.5\, w_j(t_{jv})$ is the core velocity (t_{jv} being the time at the end of the jet phase simulations; see Paoli & al. (2002)).

3.1. *Passive-particle results*

A first set of simulations was performed with the ice-growth model switched off. The object was to obtain a reference mixing case at high Reynolds numberss typical of aircraft wake configurations. It was also useful to analyze the spatial distribution of supersaturated particles and identify the regions where ice formation is most likely to occur. Basic diagnostics consists in analyzing the thermodynamic properties of the exhaust gas during mixing with ambient air. Probability Density Function (PDF) is a convenient diagnostic because it provides the additional information on the fraction of particles that supersaturate with respect to ice. Figure 5 shows the joint PDF of normalized temperature, $(T - T_a)/(T_j - T_a)$, and the partial pressure of water vapor, $(p_w - p_{w_a})/(p_{w_j} - p_{w_a})$, around soot particles. The PDF follows a straight line which indicates pure mixing between hot jet and cold air. This is a consequence of the assumptions of low Mach number and $Le = Sc/Pr = 1$.. The first assumption implies small pressure fluctuations and kinetic energy negligible compared to internal energy in (2.3). The second implies that the diffusion terms in Eqs. (2.3) and (2.4) are the same. Therefore, T and p_w are given by the same transport equations and evolve along a mixing line (obtained by elimination of r in the initial conditions, Eqs. (3.2) and (3.3))

$$\frac{p_w}{p_{w_j} - p_{w_a}} = \frac{T}{T_j - T_a} + \frac{1}{2} \left(\frac{p_{w_j} + p_{w_a}}{p_{w_j} - p_{w_a}} - \frac{T_j + T_a}{T_j - T_a} \right). \tag{3.5}$$

All particles are initially (at $t = 0.16\,s$) placed below the saturation curve p_s because they are still concentrated inside the hot jet region. Due to the mixing with cold air, particles cool, moving along the mixing line, until some of them become supersaturated (crossing of p_s curve at $t = 0.56\,s$). The spatial distribution of supersaturated particles is given in
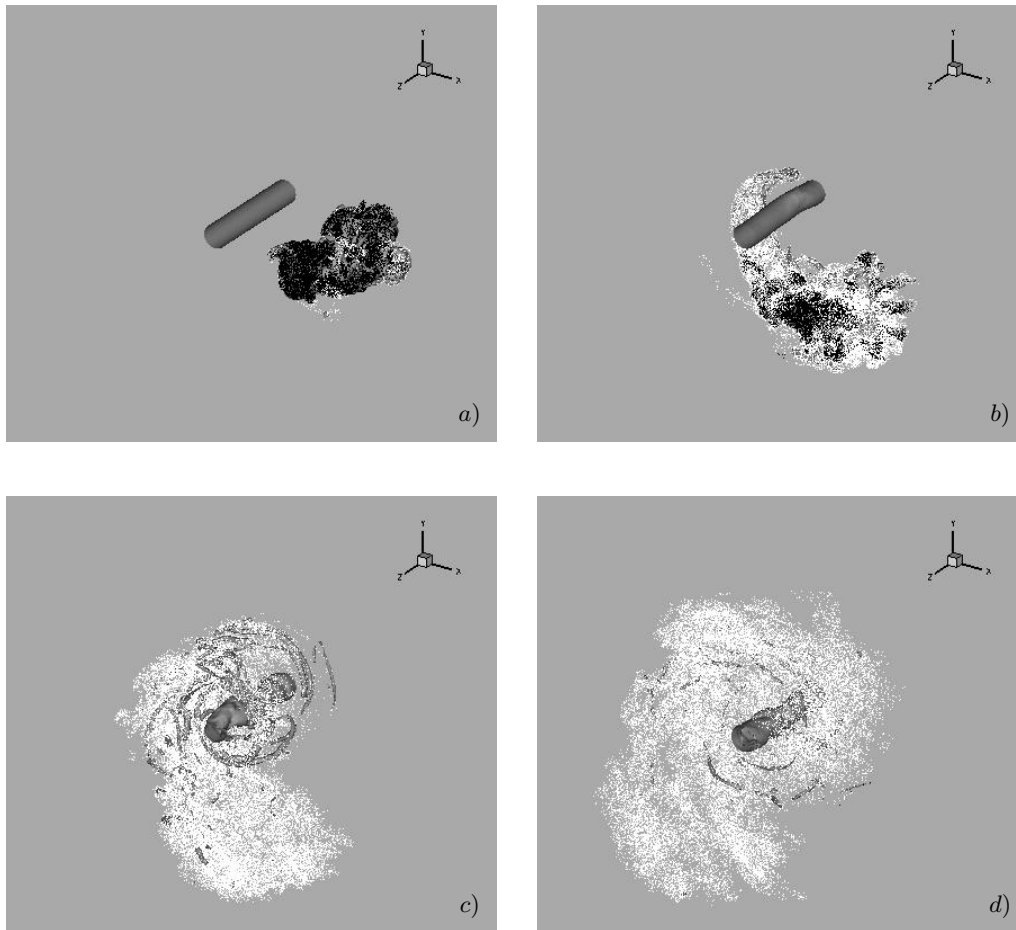
FIGURE 7. Passive particles distribution during the jet/vortex interaction phase. Dry soot particles are represented in black, iced supersaturated particles in white. Total vorticity iso-surface identifies the vortex core and the secondary vortical structures due to the interaction with the jet; a), $t = 0.7\,s$; b), $t = 1\,s$; c), $t = 1.5\,s$; d), $t = 2\,s$.

figure 6, together with a plane cut of water vapor content at two times during the jet phase. The figure shows that air first saturates around the particles placed at the edges of the jet where the temperature has fallen and there is sufficient vapor to condense.

The dynamics of the jet/vortex interaction phase are dominated by the entrainment of the jet inside the vortex field. Nevertheless, other phenomena occur, as shown in figure 7: when the jet is close enough to the vortex core, its axial velocity strongly interacts with the vortex tangential velocity, causing the formation of three-dimensional structures of azimuthal vorticity. These structures progrssively decay ($t = 2\,s$, see figure 7(d)), corresponding to complete entrainment of the jet (Paoli & *al.* (2002)). This mechanism of entrainment enhances mixing with external air: therefore, exhaust cooling and vapor condensation are favored by the presence of the vortex. Figure 7 shows that at $t = 2\,s$ all particles are supersaturated and contrail can form everywhere in the wake.
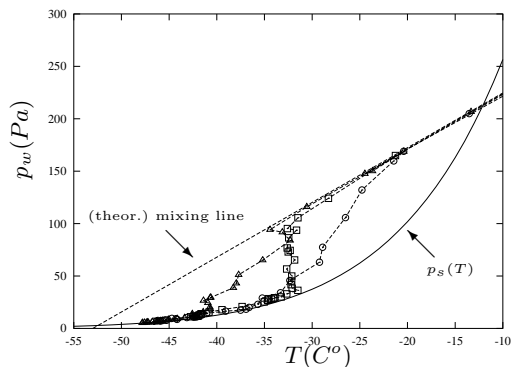
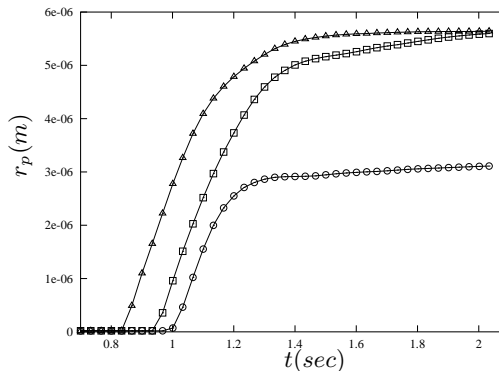FIGURE 8. Trajectories of three sample particles in a $T - p_w$ plane.

FIGURE 9. Time evolution of three sample particles radius.

3.2. *Freezing-particle results*

This section presents the results of the simulations with the ice-growth model activated. The goal is to analyze the early-stage evolution of the contrail and how it influences mixing and the thermodynamic properties of the vapor. The simulation procedure is the same as in the previous calculations, i.e., we first simulate the jet alone and then its interaction with the vortex. The key point is that the ice and vapor phases are coupled through Eqs. (2.7) and (2.8). Figure 8 displays the trajectories of three sample ice particles in the temperature/vapor-pressure plane (results are reported only during the interaction phase when ice/vapor coupling is significative). The figure shows that condensation causes large deviations from the mixing line because of vapor removal and the consequent decrease in p_w. In addition, all the particles finally collapse on the saturation curve, $p_s(T)$, which indicates the thermodynamic equilibrium between vapor and ice phases. This is confirmed in figure 9 by the evolution of ice-particle radii which attain plateau values between 3 and 6 μm. The distribution of ice crystals size is provided in figure 10 in terms of radius PDF. The peak around $r_p = r_p$ at $t = 0.7$ s (end of the jet phase) indicates that only a small amount of ice has formed. As long as ice nucleation proceeds, such a peak decreases and finally disappears, and the shape of the PDF finally approaches a Gaussian at approximatively $t = 2$ s. A remarkable result is the high variance of the PDF with $r_p'/ <r_p> \approx 0.5$. This indicates high polydispersion whereas the temperature and partial pressure around particles have become approximately uniform.

4. Future directions

The particle-tracking approach adopted in this work is an attempt to approximate the behavior of a cloud of particles by attributing the properties of a "representative" particle to all members of the cluster. In reality, however, every fluid element contains particles of many different radii due to different amounts of ice-condensation on each of them. Indeed, due to the chaotic nature of particle trajectories in a turbulent flow, particles experience quite different ambient conditions during their history. Therefore, the appropriate variable that describes the current state of the system is the distribution function of particles $n_p(r, \mathbf{x}, t)$: the number of particles of radius between 'r' and '$r + dr$' that are contained in an elementary volume '$d\mathbf{x}$' around location '$\mathbf{x}$' at time t. If the law
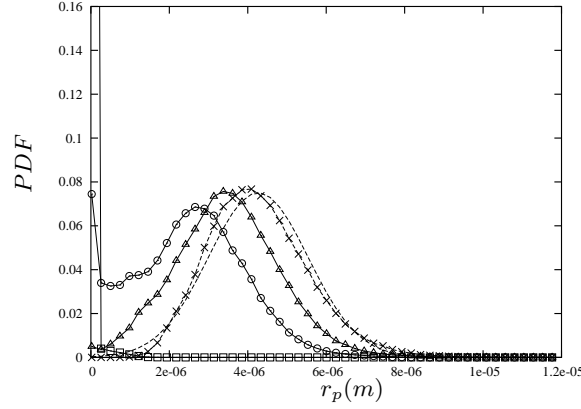
FIGURE 10. PDF of particles radius during the interaction phase; —□— , $t = 0.7\,s$; —○— , $t = 1\,s$; —△— , $t = 1.5\,s$; --×-- , $t = 2\,s$; ---- , $t = 2\,s$ (Gaussian curve).

of growth of an ice crystal, (2.7) is known, an evolution equation may be written for n_p

$$\frac{\partial n_p}{\partial t} + \nabla \cdot (n_p \mathbf{u}) = -\frac{\partial}{\partial r}(n_p \dot{r}). \tag{4.1}$$

This is essentially a Liouville equation for particle conservation in the four-dimensional phase space (x, y, z, r). The term on the right-hand side represents losses or gains from each "bin" $(r, r+dr)$ due to evaporation or condensation. The source term in the equations for mass/momentum/energy are of the form $\int_0^\infty (...)n_p\, dr$ where $(....)$ denotes the flux of the appropriate quantity onto a particle of size 'r'. In principle, one needs to simulate (4.1) for n_p, together with the equations of compressible flow. However, since solving partial differential equations in four-dimensional space involves a large increase in computational cost, it would be prudent to look for simplifying approximations. This is discussed next.

4.1. *Method of moments*

Let us assume that the size distribution of particles at a given location may be written as $n_p = F(r; m_0, m_1, \cdots)$, where m_0, m_1, $\cdots$ are parameters, which without loss of generality, may be taken as the moments of the distribution. The functional form of 'F' is presumed known. It then remains to determine evolution equations for the moments of the distribution, defined as $m_k(\mathbf{x}, t) = \int_0^\infty r^k n_p(r, \mathbf{x}, t)\, dr$. The first few moments are familiar, for example, $m_0 = N_p$, the total concentration of particles $m_1 = N_p \langle r \rangle$, where $\langle r \rangle$ is the mean size of particles; $m_2/m_0 - m_1^2/m_0^2 = \langle \Delta r^2 \rangle$, the variance of particle size distribution about the mean. If we integrate both sides of (4.1) with respect to r, we get the following equation for $m_0 = N_p$

$$\frac{\partial N_p}{\partial t} + \nabla \cdot (\mathbf{u} N_p) = 0. \tag{4.2}$$

This may also be written as $D/Dt(N_p/\rho) = 0$ using the continuity equation (D/Dt is the material derivative). It simply expresses the conservation law for the number of particles (irrespective of size). In general, on taking the r-th moment of both sides of (4.1) and using integration by parts, we have

$$\frac{\partial m_k}{\partial t} + \nabla \cdot (m_k \mathbf{u}) = \int_0^\infty n_p r^{k-1} \dot{r}\, dr. \tag{4.3}$$

The right-hand side may be evaluated if a differential equation for particle growth $\dot{r}$, and the form of the "presumed pdf" $n_p = F(r; \cdots, m_i, \cdots)$ is known. If F is assumed to be a distribution with 'n' parameters, then 'n' moment equations need to be retained.

Example 1 Let us assume the following distribution function; $n_p = N_p \delta(r - r_p)$, that is, all particles in a given fluid element at a particular time instant are identical in size. Then $m_1 \equiv N_p \langle r \rangle = N_p r_p$, and on substituting this in the moment equation (4.3) we have $\partial(N_p r_p)/\partial t + \nabla \cdot (N_p r_p \mathbf{u}) = N_p \dot{r}\,|_{r=r_p}$ which, using (4.2), may be put in the form

$$\frac{Dr_p}{Dt} = \dot{r}\,|_{r=r_p}. \tag{4.4}$$

Solving (4.4) together with $D/Dt(N_p/\rho) = 0$ is exactly equivalent to tracking a certain number of representative Lagrangian particles released into the fluid (of course, in order to obtain the exact solution an infinite number of such particles must be tracked). Particle tracking is therefore a special case of our approach.

Example 2 A more realistic model may be $n_p = N_p \phi(r; m_1, m_2)$, that is, the particle size distribution at any location is parametrized by its mean and variance. An appropriate form for ϕ may be chosen on examining the available data in the atmospheric sciences literature. Using the growth model (2.7) in (4.3) we then have the following coupled equations for determining m_1 and m_2

$$\frac{\partial m_1}{\partial t} + \nabla \cdot (m_1 \mathbf{u}) = \frac{D}{\rho_I}(Y_w - Y_s) J_1(m_1, m_2), \tag{4.5}$$

$$\frac{\partial m_2}{\partial t} + \nabla \cdot (m_2 \mathbf{u}) = \frac{D}{\rho_I}(Y_w - Y_s) J_2(m_1, m_2) \tag{4.6}$$

where ρ_I is the density of ice and J_1, J_2 are functions of m_1 and m_2 defined by

$$J_1(m_1, m_2) = \int_{r_0}^{\infty} \frac{G(r)}{r} \phi(r; m_1, m_2)\, dr, \;\; J_2(m_1, m_2) = \int_{r_0}^{\infty} G(r) \phi(r; m_1, m_2)\, dr. \tag{4.7}$$

Once the form of the presumed pdf 'ϕ', and the initial radius of soot particles, r_0, is selected, the integrals can be evaluated. Clearly, Eqs. (4.2), (4.5) and (4.6) may also be put in the Lagrangian form using the continuity equation

$$\frac{D}{Dt}\left(\frac{N_p}{\rho}\right) = 0, \tag{4.8}$$

$$\frac{D}{Dt}\left(\frac{m_1}{\rho}\right) = \frac{D}{\rho_I}\frac{Y_w - Y_s}{\rho} J_1(m_1, m_2), \tag{4.9}$$

$$\frac{D}{Dt}\left(\frac{m_2}{\rho}\right) = \frac{D}{\rho_I}\frac{Y_w - Y_s}{\rho} J_2(m_1, m_2). \tag{4.10}$$

In these equations, $\mathbf{u}$ is the velocity vector and all variables denote the physical field. In order to obtain the filtered fields, one should apply Favre averages on both sides of Eqs. (4.8) - (4.10) and introduce appropriate subgrid modeling assumptions (such as neglect of the fluctuating terms and introduction of "eddy" diffusivities) to achieve closure.

5. Conclusions

In this work, we studied the process of formation and early evolution of a contrail in the near-field of an aircraft wake. The basic tool was a two-phase flow code; the basic

configuration, an engine exhaust jet, loaded with soot particles, and interacting with a wing-tip trailing vortex. Large-eddy simulations were carried out at high Reynolds numbers, typical of wake configurations. A simple micro-physics model was used to account for nucleation of water vapor on the soot particles. A first set of simulations was carried out without any ice-growth model, to analyze the spatial distribution of supersaturation around soot particles. Results showed that particles first saturate at the edges of the exhaust jet. Vortex-induced entrainment in the wake enhances mixing of exhaust gases with cold air and favor water vapor supersaturation and condensation. A second set of simulations was carried out with the ice-growth model activated. The results showed that the radii of the frozen particles reach asymptotic values which depend on the local supersaturation. This corresponds to local thermodynamic equilibrium state between vapor and ice phases. Taking vapor depletion into account results in significant deviation from the classical mixing line. This justifies the need for two-phase flow simulations to deal with contrail formation.

6. Acknowledgments

REFERENCES

APPLEMAN, H. 1953 The formation of exhaust condensation trails by jet aircraft. *Bull. Amer. Meteor. Soc.* **34**, 14–20.

BOIVIN, M., SIMONIN O. & SQUIRES K. D. 1998 Direct numerical simulations of turbulence modulation by particles in isotropic turbulence. *J. Fluid Mech.* **375**, 235–263.

DUCROS F., COMTE P. & LESIEUR M. 1996 Large-Eddy Simulation of transition to turbulence in a boundary layer spatially developing over a flat plate. *J. Fluid. Mech.* **326**, 1–36.

GARNIER, F., BAUDOIN, C., WOODS P., & LOUISNARD, N. 1997 Engine emission alteration in the nearfield of an aircraft. *Atmos. Environ.* **31**, 1767–1781.

GARNIER, F., FERREIRA-GAGO, C. & UTHEZA, F. 2002 Numerical Investigation of turbulent mixing in a jet/wake vortex interaction. *AIAA J.* **40**, 276–284.

GIERENS, K. M. 1996 Numerical simulations of persistent contrails. *J. Atmos. Sci.* **53**, 3333–3348.

HÉLIE, J., BEDAT, B., SIMONIN, O. & POINSOT, T. J. 2002 Analysis of mixture fraction fluctuations generated by spray vaporisation. *Proc. ICNC Conference.* Sorrento (Italy). Society of Industrial and Applied Mathematics.

INTERGOVERNMENTAL PANEL OF CLIMATE CHANGE 1999 *Aviation and the Global Atmosphere.* Cambridge Univ. Press.

KARCHER, B., PETER, T., BIERMANN, U. & SCHUMANN, U. 1996 The initial composition of jet condensation trails. *J. Atmos. Sci.* **53**, 3066–3083.

LELE, S. K. 1992 Compact finite difference scheme with spectral-like resolution. *J. Comp. Phys.* **103**, 16–42.

MÉTAIS, O. & LESIEUR M. 1992 Spectral large-eddy simulation of isotropic and stably stratified turbulence. *J. Fluid Mech.* **239**, 157–194.

Paoli, R., Laporte, F., Cuenot, B., & Poinsot, T. J. 2002 Dynamics and mixing in a simple configuration of Jet/Vortex interaction. Submitted to Phys. Fluids.

Pruppacher, H. R. & J. D. Klett 1997 *Microphysics of Clouds and Precipitation.* Kluwer, Dordrecht.

Qu, X. & Davis E. J. 2001 Droplet evaporation and condensation in the near-continuum regime. *J. Aerosol Sci.* **32**, 861–875.

Schumann, U. 1996 On the conditions for contrail formation from aircraft exhausts. *Meteorol. Zeitsch.* **5**, 4–23.

Sonntag, D. 1994 Advancements in the field of hygrometry. *Meteorol. Zeitsch.* **3**, 51–66.

Travis, D. J., Carleton A. M. & Lauritsen R. G. 2002 Contrails reduce daily temperature range. *Nature* **418**, 601.